Effect of redistributed radiation on degenerate four-wave mixing

N. J. Mulgan and R. J. Ballagh
Physics Department, University of Otago, Dunedin, New Zealand
(Received 22 March 1993)

A model is formulated to investigate quantitatively how near-resonant degenerate four-wave mixing (DFWM) in a vapor of homogeneously broadened two-state atoms is affected by radiation scattered from the pump beams. The spectral intensity distribution of the scattered radiation in the interaction volume is obtained by solving the equation of radiative transfer and a detailed treatment of the modification this fluctuating field causes on the optical dipole induced by the coherent laser fields is presented. For a broad parameter regime, this modification can be expressed via a single quantity that incorporates the energy of the fluctuating field together with bandwidths and frequency offsets from the atomic resonance. Numerical solutions are given which show that the scattered field causes the DFWM reflectivity to be depressed by a significant amount, depending most strongly on a characteristic transverse length of the interaction volume. Approximate analytic expressions for the reflectivity are also given which assist in physically understanding the underlying mechanisms.
PACS number(s): 42.65.Hw

I. INTRODUCTION

Near-resonant four-wave mixing (FWM) is a tool of great practical importance in spectroscopic and diagnostic applications. A good understanding of the main features of the phenomenon has been provided by a semiclassical theory that treats the case of monochromatic lasers and incorporates saturation and atomic motion effects [1]. Considerable current interest remains, however, in the analysis of additional mechanisms which may affect the four-wave mixing process. For example, fluctuations in the pump or probe fields were shown by Cooper *et al.* [2] to produce a significant change in the dependence of the FWM reflectivity on pump power. Other workers have shown that the probe field frequency response is sensitive to the details of the relaxation mechanism. Within the framework of the optical Bloch equations, which are the basis of the usual semiclassical theory, Berman *et al.* [3] studied the effect of varying the numerical relationship between relaxation parameters in an open two-state system. In certain circumstances, however, the simple treatment of relaxation in the Bloch equations gives an inadequate description of the FWM process [4]. Singh and Agarwal [5] used modified Bloch equations to account for the correlations that may develop between strong laser fields and a collisional relaxation mechanism [6]. Wang and Steel [7], in considering the problem of spectral diffusion (transfer of excitation amongst the active radiators) developed a modified set of optical Bloch equations in which the population equations include transfer between frequency classes. Their emphasis was on describing processes in solid state materials, but their formalism (which has its roots in treatments of velocity changing collisions in atomic vapors) is rather general.

In this paper, we consider the effect that a fluctuating background radiation field produced by scattering from the laser modes can have on near-resonant degenerate four-wave mixing (DFWM). The dissipative effect of this scattering on the laser beams has been accounted for [8] within the framework of the usual near-resonant FWM theory, where the loss is quantitatively evaluated from knowledge of the Einstein A coefficient. Recently McGraw [9, 10] used fluctuation dissipation arguments to estimate the magnitude of scattering from thermal fluctuations in FWM in a Kerr medium. However, in all previous theories a scattered photon is assumed to play no further part in the FWM process. It is well known though (e.g., see Refs. [11–14]) that in resonant media, the photon can reinteract with nearby atoms. This so-called radiation trapping has been shown to have a significant effect on other nonlinear optical processes [15, 16] because of the alteration it causes in the atomic response to the laser fields.

In the simplest approach, the effect of the transport of the scattered radiation has been treated in terms of a diffusion [11] of excited state population outwards from the laser beams. Lange has used a diffusion model to gain an initial understanding of the role of radiation transport in nonlinear optics. In FWM, diffusion has also previously been used as a simple model of the effect of atomic motion [1]. However, such an approach can provide only an incomplete description of the effect of scattered radiation in FWM, where the key atomic quantity is the optical dipole, not the excited state population. In addition to exciting population transfers, the background field can, for example, dephase the dipole relative to the coherent field. To understand the effect of the scattered radiation field we must consider in detail its interaction with the atoms as well as its buildup in the atomic vapor.

In the present work we develop a specific model for four-wave mixing of monochromatic laser fields in a medium of homogeneously broadened two-state atoms, which will enable us to evaluate quantitatively the effect that scattered radiation has on the FWM process. For simplicity, we neglect velocity effects and also assume plane wave laser fields. We begin in Sec. II by

formulating an approach, based on the equation of radiative transfer, for calculating the spectral intensity of the incoherent field that develops from scattering from the counterpropagating pump fields. With the assumption that the incoherent field can be represented by a broadband chaotic stochastic process, we obtain emission and absorption coefficients appropriate for atoms driven simultaneously by both the strong monochromatic and the incoherent fields. A formal solution for the scattered field intensity distribution is then derived, incorporating the periodic character imposed on the absorption and emission coefficients by the interference pattern of the laser beams. In Sec. III we present a closed form for the polarization of atoms driven by combined monochromatic and chaotic fields, which depends on the intensity and bandwidth of the fluctuating field, and is valid in a regime where this bandwidth is sufficiently large. An analytic form is then calculated for the DFWM reflectivity in the presence of the background field, by expanding the polarization in the manner of Abrams and Lind [17]. In Sec. IV we calculate numerically a self-consistent solution to the background intensity distribution, and show its dependence on the volume of the interaction region. We are then able to verify that this field meets various of the validity conditions that we imposed in the formal derivation of the theory. Simple analytic estimates are given of the background intensity term needed in the DFWM reflectivity, that agree well with the numerical results. Finally, in Sec. V, we present numerical results for the DFWM reflectivity, for laser fields both on and off resonance, and discuss its dependence on pump intensity and the length and volume of the interaction region. An analytic approximation for the reflectivity is given that enables us to make simple estimates of the influence of the scattered field.

II. TRANSFER OF SCATTERED RADIATION

Formulation of treatment

We consider for our model a medium consisting of homogeneously broadened two-state atoms which have frequency ω_0, dipole matrix element $\mathbf{d}$, and transverse and longitudinal decay rates Γ and γ, respectively. Two strong pump fields of frequency ω_ℓ,

$$\mathbf{E}_f = \mathcal{E}_f(z)\, E_{\rm sat}\, \hat{\mathbf{e}}\, e^{i(kz-\omega_\ell t)} + \text{c.c.}$$

and (1)

$$\mathbf{E}_b = \mathcal{E}_b(z)\, E_{\rm sat}\, \hat{\mathbf{e}}\, e^{i(-kz-\omega_\ell t)} + \text{c.c.},$$

propagate through the medium in the forward and backward directions, respectively, and their slowly varying positive frequency amplitudes $\mathcal{E}_f$ and $\mathcal{E}_b$ are expressed in units of $E_{\rm sat}$, the saturation field amplitude,

$$E_{\rm sat} = \frac{\hbar\,(\Gamma\gamma)^{1/2}}{2\,\mathbf{d}\cdot\hat{\mathbf{e}}}. \tag{2}$$

The forward and backward beams form a standing wave pattern in the medium, with positive frequency amplitude

$$\mathcal{E}_0(z) = \mathcal{E}_f(z)e^{ikz} + \mathcal{E}_b(z)e^{-ikz}, \tag{3}$$

and grating spacing Λ, so we choose $k = \pi/\Lambda$ as the most convenient choice of wave vector in Eq. (1). The Rabi frequency at any spatial point is given by

$$\Omega = (\Gamma\gamma)^{1/2}\,\mathcal{E}_0(z), \tag{4}$$

and the corresponding intensity I, which is given in units of the saturation intensity $I_{\rm sat} = 2\,\epsilon_0\,c\,E_{\rm sat}^2$, is

$$I = |\Omega|^2/\Gamma\gamma, \tag{5}$$

where the z dependence in Ω and I is understood. As the pump beams propagate through the medium, energy is lost from the pump modes, and is redistributed into other modes by scattering from the atomic medium. The scattered radiation forms a fluctuating background field which propagates through the medium in all directions, modifying the atomic response to coherent fields, and thus affecting the four-wave mixing process. We represent this incoherent background field by

$$\mathbf{E}^{\rm inc}(\mathbf{r},t) = \sum_{j=x,y,z} \hat{\mathbf{e}}_j\, E_{\rm sat}\left[\mathcal{E}_j^{\rm inc}(\mathbf{r},t)\, e^{-i(\omega_0+\Delta_c)t} + \text{c.c.}\right], \tag{6}$$

where $\hat{\mathbf{e}}_j$ is the unit vector in the j direction and we have assumed a band-center frequency $\omega_0 + \Delta_c$. We expect the background field to be well represented by a chaotic Markovian field [18,19] and so we model the stochastic behavior by assuming the $\mathcal{E}_j^{\rm inc}(\mathbf{r},t)$ are independent stationary chaotic Markovian processes, each with the same bandwidth b and with correlation relations given by

$$\left\langle \mathcal{E}_j^{\rm inc}(\mathbf{r},t_1)[\mathcal{E}_k^{\rm inc}(\mathbf{r},t_2)]^* \right\rangle$$

$$= \delta_{jk}\left\langle \mathcal{E}_j^{\rm inc}(\mathbf{r},t_1)[\mathcal{E}_k^{\rm inc}(\mathbf{r},t_1)]^* \right\rangle e^{-b|t_2-t_1|}. \tag{7}$$

Under the additional assumption of isotropy of the background field, the variance of each polarization component of the field is identical, and we define the rms Rabi frequency for each polarization as

$$\overline{\Omega}_c \equiv \sqrt{\Gamma\gamma\left\langle \mathcal{E}_j^{\rm inc}(\mathbf{r},t)[\mathcal{E}_j^{\rm inc}(\mathbf{r},t)]^* \right\rangle} \tag{8}$$

(for any value of j), where the $\mathbf{r}$ dependence of $\overline{\Omega}_c$ is understood. The response function for an atom driven coherently in the presence of such a fluctuating field has previously been derived [15, 20]. In general the evaluation of the response function is computationally intensive but, if the mean Rabi frequency of the background field is less than its bandwidth ($\overline{\Omega}_c < b$), a decorrelation approximation can be made, and an explicit form requiring only the value of the coherent field, and the intensity distribution of the background radiation, can be used. In Sec. IV we show that the decorrelation condition is met for the cases we consider, and so for our purposes sufficient characterization of the background radiation is contained in its specific intensity I_ω (intensity at frequency ω

per unit bandwidth per unit solid angle), whose buildup is described by the equation of radiative transfer [21]. Of course, before the transfer equation can be solved, the geometry of the interaction region must be known, and for definiteness we shall assume that the pump beams occupy a cylinder of radius r_0 and length ℓ within the medium (see Fig. 1), and for simplicity we will assume that within this cylinder the pump fields have plane wave fronts, and uniform intensity across the wave fronts [22]. It is convenient to set up a coordinate system where each ray through the cylinder has a label ρ, and the distance along a ray is labeled η, where $\eta = 0$ is the point where the ray enters the cylinder (see Fig. 1). The (steady-state) equation for radiative transfer of the incoherent radiation can now be expressed [in SI (Système International) units] as [21]

$$\frac{dI_\omega(\rho,\eta)}{d\eta} = j_\omega(\rho,\eta) - \kappa_\omega(\rho,\eta) I_\omega(\rho,\eta). \tag{9}$$

Here j_ω and κ_ω, the emission and absorption coefficients for radiation of frequency ω propagating along ρ, depend on the strong coherent fields (the pumps) and in principle, also on the weaker probe and conjugate fields, as well as the background radiation itself. A complete solution incorporating all of these dependencies is, for practical purposes, intractable, since it involves the nonlinear and nonlocal coupling of the transfer equation with the Maxwell Bloch equation for the coherent fields. Fortunately, for the situation we consider here, simplifying approximations can be made. When the probe and conjugate beams are much weaker than the pump beams, the effect of the probe and conjugate can be neglected [23] in the calculation of j_ω and κ_ω. Using this assumption, Mollow [25] has derived emission and absorption coefficients for atoms in the presence of a coherent field (i.e., the pumps), in the absence of a background field. We present his results immediately below, and later [see Eq. (20) *et seq.*] give simple modifications, valid in the decorrelation regime, that account for the additional effect of a fluctuating background field. Mollow's results, given here after some simplifying algebra and with appropriate normalization are, in SI units,

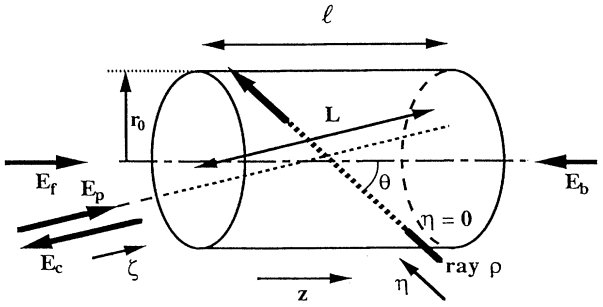

FIG. 1. Geometry of the FWM interaction region, showing the direction of propagation of each coherent field, and a typical path ρ for the incoherent radiation transfer.

$$\kappa_\omega = -\alpha_0 n \Gamma \,\mathrm{Re}\left\{ \frac{1}{D}\left((-i\Delta_s + \gamma)[i(\Delta - \Delta_s) + \Gamma] + \frac{i|\Omega|^2 \Delta_s}{2(i\Delta + \Gamma)} \right) \right\} \tag{10}$$

and

$$j_\omega = \frac{\alpha_0 n_u I_{\mathrm{sat}}}{4\pi^2} f_{\mathrm{inc}} \{ (2\Gamma - \gamma)(\Delta_s{}^2 + \gamma^2)[\Gamma^2 + (\Delta - \Delta_s)^2] + |\Omega|^2 [\gamma^2 \Delta(\Delta_s - \Delta)/\Gamma + \gamma[2(\Delta - \Delta_s)^2 + \Delta\Delta_s + 4\Gamma^2] + 2\Gamma\Delta_s(\Delta - \Delta_s) + \Gamma|\Omega|^2]\}/|D|^2, \tag{11}$$

where

$$f_{\mathrm{inc}} = 1 - \frac{\gamma}{2\Gamma}\left\{ 1 + \frac{\Gamma|\Omega|^2}{\gamma(\Gamma^2 + \Delta^2)} \right\}^{-1} \tag{12}$$

and

$$D = (-i\Delta_s + \gamma)[i(\Delta - \Delta_s) + \Gamma][-i(\Delta + \Delta_s) + \Gamma] + |\Omega|^2(-i\Delta_s + \Gamma). \tag{13}$$

In these expressions, α_0 is the weak field absorption coefficient,

$$\alpha_0 = \frac{N}{V} 3 \frac{\gamma}{\Gamma} \pi \left(\frac{c}{\omega}\right)^2, \tag{14}$$

where N/V is the number density of atoms, n is the atomic inversion (for a single atom),

$$n = -\left\{ 1 + \frac{|\Omega|^2}{\Gamma\gamma(1 + \Delta^2/\Gamma^2)} \right\}^{-1}, \tag{15}$$

n_u is the upper state population (for a single atom), and the detunings are

$$\Delta_s = \omega - \omega_l, \tag{16}$$

$$\Delta = \omega_l - \omega_0. \tag{17}$$

We note that j_ω describes only the incoherent scattering, while the coherent scattering that also occurs and is represented by an additional δ function in Mollow's emission spectrum would be treated in the coherent Maxwell-Bloch propagation equation for the laser field rather than the transfer equation Eq. (9). The quantity f_{inc} is the incoherent fraction of the total intensity scattered by the atom and, for pure radiative broadening, ($\Gamma = \gamma/2$) is zero at low laser power. The emission and absorption coefficients are normalized such that

$$\int_{-\infty}^{\infty} \kappa_\omega d\omega = -\alpha_0 n \Gamma \pi, \tag{18}$$

$$\int_{-\infty}^{\infty} j_\omega d\omega = \alpha_0 n_u I_{\mathrm{sat}} f_{\mathrm{inc}}/2\pi. \tag{19}$$

When an isotropic fluctuating background field is also

present, with effective intensity per unit bandwidth U_b, where

$$U_b = 3\frac{\overline{\Omega}_c^2}{\gamma(\Gamma+b)}\left(1+\frac{\Delta_c^2}{(\Gamma+b)^2}\right)^{-1}, \tag{20}$$

then in the decorrelation approximation the absorption and emission coefficients have the same form as Eq. (10) and Eq. (11), but with the inversion given by [24]

$$n = -\left\{1+\frac{|\Omega|^2}{\Gamma\gamma(1+\Delta^2/\Gamma^2)}+U_b\right\}^{-1}, \tag{21}$$

and $n_u = (n+1)/2$.

Behavior of j_ω and κ_ω

The emission and absorption coefficients are crucial in determining the background radiation, and in this section we summarize their main features. A somewhat more detailed discussion is given in the Appendix.

In Fig. 2 the frequency dependence of j_ω for the case of strong collisional broadening ($\Gamma \gg \gamma$) is plotted for a range of pump Rabi frequencies, with the pump both on resonance ($\Delta = 0$) and off resonance ($\Delta = 5\Gamma$). We can see, and Mollow [26] has shown, that in general (when $\Omega > \Gamma$ or $\Delta > \Gamma$) the emission coefficient consists of three Lorentzian peaks, one at the laser frequency ω_l with the others at $\omega_l \pm \Omega'$, where the generalized Rabi frequency is

$$\Omega' = \sqrt{\Omega^2+\Delta^2}. \tag{22}$$

When $|\Delta| > \Omega, \Gamma$, in the collisionally broadened case most of the scattered intensity is in the peak centered nearest the atomic frequency, and j_ω is well described by

$$j_\omega \to \frac{\alpha_0 n_u I_{\rm sat}}{4\pi^2} f_{\rm inc}\frac{(2\Gamma-\gamma)}{(\Delta+\Delta_s)^2+\Gamma^2}. \tag{23}$$

This single Lorentzian also accurately describes j_ω in the resonant case ($\Delta = 0$) at sufficiently low power ($\Omega \leq \gamma$). However, at resonance in the collisionally broadened case, a dip develops at line center as the Rabi frequency increases, and eventually j_ω becomes three Lorentzian peaks of equal height.

In Fig. 3 the frequency dependence of κ_ω is plotted for a similar range of parameters to those in Fig. 2. At low power, the profile is a Lorentzian centered at the atomic frequency. For a resonant pump field, a dip of width

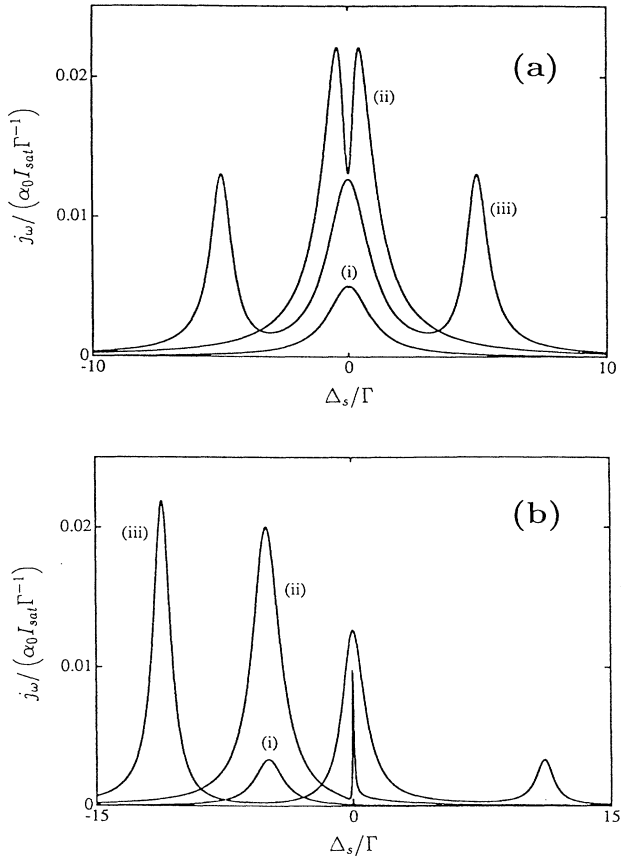

FIG. 2. The emission coefficient j_ω as a function of the scattered frequency for (a) $\Delta = 0$ with (i) $\Omega = 0.05\Gamma$, (ii) $\Omega = 0.5\Gamma$, (iii) $\Omega = 5\Gamma$, and (b) $\Delta = 5\Gamma$ with (i) $\Omega = 0.2\Gamma$, (ii) $\Omega = \Gamma$, (iii) $\Omega = 10\Gamma$. For each graph $\gamma = 0.01\Gamma$.

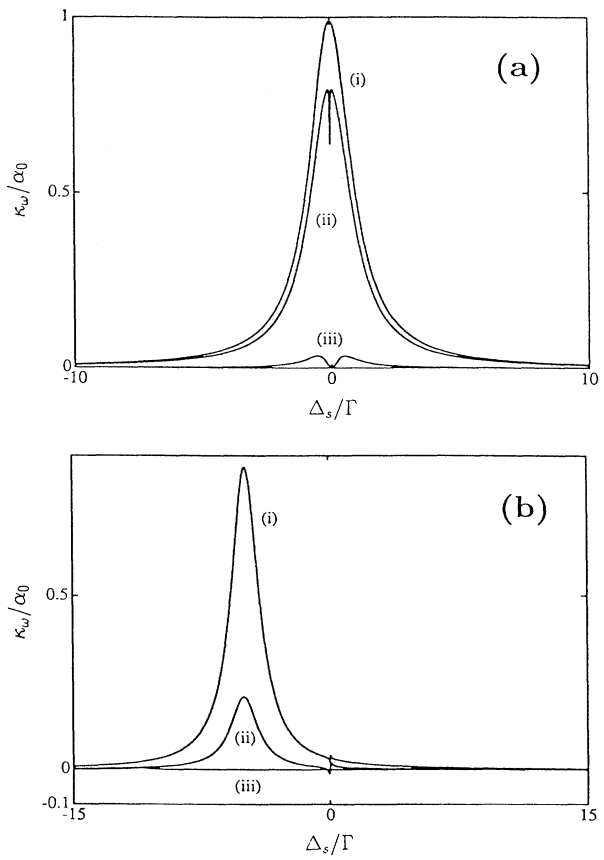

FIG. 3. The absorption coefficient κ_ω as a function of the incident frequency for (a) $\Delta = 0$ with (i) $\Omega = 0.01\Gamma$, (ii) $\Omega = 0.05\Gamma$, (iii) $\Omega = 0.5\Gamma$, and (b) $\Delta = 5\Gamma$ with (i) $\Omega = 0.2\Gamma$, (ii) $\Omega = \Gamma$, (iii) $\Omega = 10\Gamma$. For each graph $\gamma = 0.01\Gamma$.

$\sim \Omega$ appears at the center of the line as the pump power increases (and may eventually give regions of gain if Ω is large enough). The origin of this dip has been attributed to "coherent population oscillation" by Lee *et al.* [27] and further discussed by Boyd *et al.* [28]. Off resonance ($\Delta \geq \Gamma$), the absorption profile is asymmetric, but provided $\Omega \leq \Delta$, the dominant part of κ_ω can be described by a Lorentzian centered at the sideband nearest the atomic resonance frequency, namely

$$\kappa_\omega \underset{\Delta \geq \Gamma, \Omega}{\longrightarrow} -\alpha_0 n \Gamma \frac{\Gamma}{(\Delta_s + \frac{\Delta}{|\Delta|}\Omega')^2 + \Gamma^2}. \tag{24}$$

A small amount of gain may appear near the laser frequency, adjacent to a region of absorption, and as Ω increases beyond Δ, gain may also appear at the far sideband. For all cases the peak value of κ_ω, which occurs at $\Delta_s \approx -(\Delta/|\Delta|)\Omega'$ (or $\Delta_s \approx \pm\Omega$ if $\Delta = 0$), is of order $-\alpha_0 n$.

Procedure for calculating I_ω

The scattered radiation propagates (in all directions) through the standing wave grating formed by the pumps and since $\kappa_\omega \Lambda$ is small, the length scale for attaining a constant background field is typically many grating wavelengths [see also Eq. (30)]. If we assume the pump field amplitudes $\mathcal{E}_f$ and $\mathcal{E}_b$ are independent of z, then the coefficients j_ω and κ_ω are periodic along any ray ρ, with period $\lambda_\rho = \Lambda/\cos\theta$ (where θ is the angle of the ray to the z axis), and the transfer equation can be solved in a simple manner as we show below. Strictly, of course, the forward and backward pump fields must diminish as they propagate but, as we show in Sec. IV, for sufficiently large initial $\mathcal{E}_f$ and $\mathcal{E}_b$ the relative variation of the standing wave peak intensities along a path ρ will be unimportant, and so our model gives a good representation of the buildup of the background field. Choosing $\mathcal{E}_f = \mathcal{E}_b$, and the boundary condition for each ray as

$$I_\omega(\rho, \eta = 0) = 0 \tag{25}$$

(which amounts to assuming that radiation leaving the interaction region is not returned), the solution for I_ω at integral values of λ_ρ is given by

$$I_\omega(\rho, \eta = m\lambda_\rho) = \left(1 - e^{-m\bar{\kappa}_\omega \lambda_\rho}\right) I_\omega(\rho, \eta = \infty). \tag{26}$$

Here $\bar{\kappa}_\omega$ is the average absorption coefficient over one period along the path,

$$\bar{\kappa}_\omega = \frac{1}{\lambda_\rho} \int_0^{\lambda_\rho} \kappa_\omega(\rho, \eta)\, d\eta. \tag{27}$$

The path dependence ρ in the integrand enters through the variation of $|\Omega|^2$, and $\bar{\kappa}_\omega$ is easily seen to be independent of ρ, i.e., independent of the direction the transfer ray takes through the standing wave. The asymptotic [29] intensity is given by

$$I_\omega(\rho, \eta = \infty) = \frac{\lambda_\rho \bar{j}_\omega(\rho)}{1 - e^{-\bar{\kappa}_\omega \lambda_\rho}}, \tag{28}$$

where $\bar{j}_\omega$ is the net emission coefficient over one period along the path,

$$\bar{j}_\omega(\rho) = \frac{1}{\lambda_\rho} \int_0^{\lambda_\rho} \exp\left\{-\int_\eta^{\lambda_\rho} \kappa_\omega(\rho, \eta')\, d\eta'\right\} j_\omega(\rho, \eta)\, d\eta. \tag{29}$$

Expressions (26)–(29) form the basis for the numerical calculation of the background radiation that is presented in Sec. IV. Before proceeding numerically, it is useful to make approximate estimates of $\bar{\kappa}_\omega$ and $\bar{j}_\omega$. Using the approximate peak value for κ_ω of $-\alpha_0 n$ in Eq. (27), we obtain a measure of the peak value of $\bar{\kappa}_\omega$,

$$(\bar{\kappa}_\omega)_{\text{peak}} \approx \alpha_0 \left[\frac{1}{\sqrt{(1 + U_b)(1 + U_b + \mathcal{I}_m)}}\right], \tag{30}$$

where

$$\mathcal{I}_m = \frac{I_{\max}}{1 + \Delta^2/\Gamma^2}, \tag{31}$$

and $I_{\max}$ is the intensity of the pump field at the antinodes of the standing wave. This value for the peak provides a useful guide, but is not highly accurate since the center frequency of the peak will move as the pump field varies through the standing wave. For strong resonant pumps, the absorption profile is significantly depressed in its central region, and a more representative estimate of the $\bar{\kappa}_\omega$ may be obtained by using the line center value Eq. (A3) of κ_ω in Eq. (27). For $I_{\max} > 1$ the result for $\bar{\kappa}_\omega$, on resonance, can be accurately approximated as

$$\bar{\kappa}_{\omega_0} \approx \frac{\alpha_0}{U_b \sqrt{I_{\max}}} \left[1 - \frac{1}{\sqrt{1 + U_b}}\right] \quad (\Delta = 0, \Delta_s = 0). \tag{32}$$

Equation (30) and Eq. (32) show explicitly that the absorption decreases as the pump intensity increases, and is small over a grating period for typical values of α_0 (since $\alpha_0 \Lambda \ll 1$).

For resonant pumps we can similarly estimate $\bar{j}_\omega$ at line center, approximating j_ω by Eq. (A4) and using the fact that $\int_\eta^{\lambda_\rho} \kappa_\omega(\rho, \eta')\, d\eta'$ in Eq. (29) is at most of order $\lambda_\rho \alpha_0$ so that (for almost all rays except those with $\theta \approx 90°$) the integrand in Eq. (29) becomes simply j_ω and

$$\bar{j}_{\omega_0} \approx \frac{\alpha_0 I_{\text{sat}} f_{\text{inc}}}{8\Gamma\pi^2} \left[1 + \frac{U_b - 1}{\sqrt{(1 + U_b)(1 + U_b + 2I_{\max})}}\right] \quad (\Delta = 0, \Delta_s = 0). \tag{33}$$

For a low level of background field ($U_b < 1$), $\bar{j}_{\omega_0}$ is small at small $I_{\max}$ and increases with $I_{\max}$ to the saturated value $\alpha_0 I_{\text{sat}} f_{\text{inc}}/8\Gamma\pi^2$. Even for very large U_b, the saturated value of $\bar{j}_{\omega_0}$ can be no more than twice this value. In the line wings [i.e., where Eq. (A1) applies through most of a standing wave period] Eq. (23) can be used to approximate $\bar{j}_\omega$ as

$$\bar{j}_\omega \approx \frac{\alpha_0 I_{\text{sat}} f_{\text{inc}}}{8\pi^2} \left[1 - \frac{1}{\sqrt{(1 + U_b)(1 + U_b + I_{\max})}}\right] \times \frac{(2\Gamma - \gamma)}{(\Delta + \Delta_s)^2 + \Gamma^2}. \tag{34}$$

We can see from Eqs. (32)–(34) that $\bar{\kappa}_\omega$ and $\bar{j}_\omega$ have only a small effect over any single period of the standing wave grating, and it is a good approximation to interpolate the periodic solution of Eq. (26) for I_ω to all values of η, writing

$$I_\omega(\rho,\eta) = \left(1 - e^{-\bar{\kappa}_\omega \eta}\right) I_\omega(\rho, \eta = \infty). \tag{35}$$

When $\bar{\kappa}_\omega \eta$ is small (as it may be for large pump intensity or in the wings of the line, in a finite medium) then

$$I_\omega \approx \eta \bar{j}_\omega, \tag{36}$$

so that for many cases (and the ones of interest in this paper) the background radiation will build up appreciably only in the vicinity of line center (where $\bar{j}_\omega$ is largest), and will eventually fall off with Lorentzian wings. The atom response function is, in our model (see Sec. III), affected equally by background radiation coming from all directions, so we require at each point the integral of I_ω over all angles, which is called the total specific intensity,

$$I_\omega^{\rm tot} = \int_{4\pi} I_\omega \, d\Omega. \tag{37}$$

On the basis of Eq. (36), we expect that $I_\omega^{\rm tot}$ can be represented by a single Lorentzian, or perhaps (at large pump intensity) the sum of Lorentzians. In Sec. IV we perform detailed numerical calculations to obtain $I_\omega^{\rm tot}$.

We note that in our calculation of the transferred radiation, we have used κ_ω and j_ω in isotropic (angle averaged) form, even though in more detail they will depend on the relative direction of the pump polarization and the transfer ray being considered. The main reason for our choice is that the model we will use (in Sec. III) to determine the altered atomic response function to the coherent fields requires only the angular integrated value of the background radiation $I_\omega^{\rm tot}$. We will also find, in Sec. IV, that four-wave mixing is not sensitive to small changes in $I_\omega^{\rm tot}$, such as we could expect from using angularly dependent rather than isotropic forms of κ_ω and j_ω in the transfer equation.

III. FOUR-WAVE MIXING WITH BACKGROUND FIELD

The four-wave mixing behavior for atoms with a fluctuating background radiation field can be calculated by the same method as is used in simpler systems (with no background field), since the underlying physical mechanism for the mixing is the same: a macroscopic polarization grating is induced by the three coherent input fields, which thereby generates the fourth (conjugate) field. The effect of the fluctuating background field will be accounted for in the modification it makes to the atomic dipole, and hence the coherent polarization grating. A simple characterization of the overall effect of the background field on the four-wave mixing process is given by the reflectivity of the probe beam. For degenerate four-wave mixing, the reflectivity R can be calculated once the response function to a single coherent frequency is known, using the method of Abrams and Lind [17]. In this paper we consider only DFWM, and we begin by calculating the response of a two-state atom driven by both a strong coherent field and a fluctuating background field.

Macroscopic polarization

The polarization $\mathbf{P_0}$ of the atoms subject to a coherent field of positive frequency amplitude $\mathcal{E}_0$ [see Eq. (3)], and the chaotic Markovian background field of Eq. (6), can be found using a method based on that developed by Zoller [30] and Georges [31]. In general the solution is given in terms of an infinite two-dimensional recurrence relation [Eq. (4.94) [20]] which must be truncated at some finite point and solved numerically. However, if the condition

$$\overline{\Omega}_c < b \tag{38}$$

is satisfied, where $\overline{\Omega}_c$ is a mean Rabi frequency and b is the halfwidth of the Lorentzian spectrum of the background field, a decorrelation approximation can be made which allows the recurrence relation to be terminated after the first few terms. Generalizing previous results [15, 20] to include arbitrary Δ_c, we obtain the macroscopic polarization

$$\mathbf{P_0} = \mathcal{P}_0 \hat{\mathbf{e}} e^{-i\omega_\ell t} + \text{c.c.}, \tag{39}$$

where

$$\mathcal{P}_0 = -i\epsilon_0 \alpha_0 \frac{c}{\omega_\ell} E_{\rm sat} \frac{1}{1 - i\Delta/\Gamma} \mathcal{E}_0 n \{1 - T_b\}, \tag{40}$$

with ϵ_0 the permittivity of free space,

$$T_b = 3\overline{\Omega}_c^2 \left(\frac{1}{\gamma + b + i\Delta_c} + \frac{1}{\Gamma - i\Delta} \right) D_b^{-1}, \tag{41}$$

$$D_b = 2\left[\gamma + b + i(\Delta_c - \Delta)\right] + \Gamma\gamma|\mathcal{E}_0|^2 \left(\frac{1}{\gamma + b + i\Delta_c} + \frac{1}{\gamma + b + i(\Delta_c - 2\Delta)} \right) + 3\overline{\Omega}_c^2 \left(\frac{2}{\Gamma + 2b + i(2\Delta_c - \Delta)} + \frac{1}{\Gamma + 2b + i\Delta} + \frac{1}{\Gamma - i\Delta} \right), \tag{42}$$

and n the inversion,

$$n = -\left\{ 1 + \frac{|\mathcal{E}_0|^2}{1 + \Delta^2/\Gamma^2} + U_b - V \right\}^{-1}. \tag{43}$$

Here U_b, the background radiation saturation term, is given by

$$U_b = \frac{\int_{-\infty}^{\infty} I_\omega^{\rm tot} \, d\omega}{(1 + b/\Gamma) I_{\rm sat}} \left(1 + \frac{{\Delta_c}^2}{(\Gamma + b)^2} \right)^{-1}, \tag{44}$$

where we have used

$$\overline{\Omega}_c^2 = \frac{\Gamma\gamma}{3I_{\rm sat}} \int_{-\infty}^{\infty} I_\omega^{\rm tot}\, d\omega, \tag{45}$$

in Eq. (20), and

$$V = \Gamma|\mathcal{E}_0|^2 {\rm Re}\left\{\left(\frac{1}{\gamma + b + i\Delta_c} + \frac{1}{\Gamma - i\Delta}\right) T_b\right\}. \tag{46}$$

If in addition to the decorrelation condition Eq. (38), the following conditions also hold:

$$\overline{\Omega}_c^2 \ll b\Gamma, \tag{47}$$

$$\Gamma, b \gg \gamma, \tag{48}$$

then T_b and V may be neglected, further simplifying the result to

$$\mathcal{P}_0 \simeq -i\epsilon_0\alpha_0 \frac{c}{\omega_\ell} E_{\rm sat} \frac{1}{1 - i\Delta/\Gamma} \mathcal{E}_0 n \tag{49}$$

$$\simeq i\epsilon_0\alpha_0 \frac{c}{\omega_\ell} E_{\rm sat} \frac{1}{1 - i\Delta/\Gamma} \mathcal{E}_0 \left\{1 + \frac{|\mathcal{E}_0|^2}{1 + \Delta^2/\Gamma^2} + U_b\right\}^{-1}, \tag{50}$$

which is the expression we will begin with when calculating the DFWM reflectivity (see also [15]). The background field now enters the response function only through U_b in the denominator of Eq. (50), and when $U_b = 0$ we regain the standard response of two-state atoms to a coherent field alone. For $U_b \neq 0$ the saturation behavior is modified.

It is interesting to note that Eq. (50) can be obtained from the standard two-state form by making the substitution $\gamma \to \gamma'$ everywhere (including in α_0 and $E_{\rm sat}$), where

$$\gamma' = \frac{\gamma}{1 + \dfrac{U_b[1 + (\Delta/\Gamma)^2]}{|\mathcal{E}_0|^2}}. \tag{51}$$

Similarly substituting $N/V \to (N/V)'$ in α_0, where

$$\left(\frac{N}{V}\right)' = \frac{N/V}{1 + \dfrac{U_b}{1 + |\mathcal{E}_0|^2/[1 + (\Delta/\Gamma)^2]}}, \tag{52}$$

will also produce Eq. (50) from the standard two-state form. A physical interpretation of the structure of Eq. (51) or Eq. (52) is not immediately apparent; nevertheless the reduction of either the population decay rate or the effective density, due to the background radiation, is intuitively appealing.

In some cases, when the pump intensity is very large, the background field may be better represented as two separated Lorentzians. We would then write

$$\mathbf{E}^{\rm inc}(\mathbf{r}, t) = \sum_{j=x,y,z} \hat{\mathbf{e}}_j\, E_{\rm sat} \left\{\left[\mathcal{E}_{1_j}^{\rm inc}(\mathbf{r}, t) e^{-i\Delta_{c1}t} + \mathcal{E}_{2_j}^{\rm inc}(\mathbf{r}, t) e^{-i\Delta_{c2}t}\right] e^{-i\omega_0 t} + {\rm c.c.}\right\}, \tag{53}$$

where the chaotic Markovian processes $\mathcal{E}_{1_j}^{\rm inc}$ and $\mathcal{E}_{2_j}^{\rm inc}$ have correlation properties

$$\left\langle \mathcal{E}_{i_j}^{\rm inc}(\mathbf{r}, t_1)[\mathcal{E}_{i_k}^{\rm inc}(\mathbf{r}, t_2)]^* \right\rangle = \delta_{jk} \frac{\overline{\Omega}_{ci}^2}{\Gamma\gamma} e^{-b_i|t_2 - t_1|}, \tag{54}$$

$$\left\langle \mathcal{E}_{1_j}^{\rm inc}(\mathbf{r}, t_1)[\mathcal{E}_{2_k}^{\rm inc}(\mathbf{r}, t_2)]^* \right\rangle = 0. \tag{55}$$

Provided the conditions Eq. (38), Eq. (47), and Eq. (48) hold for both b_1 and b_2 in place of b, we can again obtain the simplified equation for the polarization given in Eq. (50) but with U_b generalized to

$$U_b = \frac{3\overline{\Omega}_{c1}^2}{\gamma(\Gamma + b_1)} \left(1 + \frac{{\Delta_{c1}}^2}{(\Gamma + b_1)^2}\right)^{-1} + \frac{3\overline{\Omega}_{c2}^2}{\gamma(\Gamma + b_2)} \left(1 + \frac{{\Delta_{c2}}^2}{(\Gamma + b_2)^2}\right)^{-1}, \tag{56}$$

which could be readily rewritten in terms of the total intensity using

$$\overline{\Omega}_{c1}^2 + \overline{\Omega}_{c2}^2 = \frac{\Gamma\gamma}{3I_{\rm sat}} \int_{-\infty}^{\infty} I_\omega^{\rm tot}\, d\omega. \tag{57}$$

DFWM reflectivity

Degenerate four-wave mixing occurs when a coherent probe field,

$$\mathbf{E}_p = \mathcal{E}_p(\zeta)\, E_{\rm sat}\, \hat{\mathbf{e}} e^{i(k\zeta - \omega_\ell t)} + {\rm c.c.}, \tag{58}$$

propagating in a direction ζ (see Fig. 1) with the same frequency as the pump fields gives rise to a coherent conjugate field,

$$\mathbf{E}_c = \mathcal{E}_c(\zeta)\, E_{\rm sat}\, \hat{\mathbf{e}} e^{i(-k\zeta - \omega_\ell t)} + {\rm c.c.} \tag{59}$$

In units of $E_{\rm sat}$, the total positive frequency coherent field amplitude is

$$\mathcal{E} = \mathcal{E}_0 + \mathcal{E}_1, \tag{60}$$

where $\mathcal{E}_0$ is given by Eq. (3) and

$$\mathcal{E}_1 = \mathcal{E}_p(\zeta) e^{ik\zeta} + \mathcal{E}_c(\zeta) e^{-ik\zeta}. \tag{61}$$

The positive frequency polarization amplitude, $\mathcal{P}$, induced by these fields, is given by Eq. (50) with $\mathcal{E}$ in place of $\mathcal{E}_0$. Following Abrams and Lind [17] we expand $\mathcal{P}$ about $\mathcal{E} = \mathcal{E}_0$ and to first order in $\mathcal{E}_1$ write

$$\mathcal{P} = \mathcal{P}_0 + \frac{i\epsilon_0\alpha_0 \dfrac{c}{\omega_\ell} E_{\rm sat} \dfrac{1}{1 - i\Delta/\Gamma} \left[\mathcal{E}_1 (1 + U_b) - \mathcal{E}_1^* \dfrac{{\mathcal{E}_0}^2}{1 + \Delta^2/\Gamma^2}\right]}{\left\{1 + \dfrac{|\mathcal{E}_0|^2}{1 + \Delta^2/\Gamma^2} + U_b\right\}^2}. \tag{62}$$

Using this expression for $\mathcal{P}$, the propagation equations for $\mathcal{E}_p(\zeta)$ and $\mathcal{E}_c(\zeta)$ can now be derived using the same method and initial conditions as Abrams *et al.* [1]. The probe field has an interaction length L in the medium (see Fig. 1), and solving the coupled equations for the values of $\mathcal{E}_p$ and $\mathcal{E}_c$ at the input position for the probe field gives the following expression for the DFWM reflectivity:

$$R = \left|\frac{\mathcal{E}_c(0)}{\mathcal{E}_p(0)}\right|^2 = \left|\frac{\beta \sin(\sigma L)}{\sigma\cos(\sigma L) + \alpha_p \sin(\sigma L)}\right|^2, \tag{63}$$

where the probe and conjugate (amplitude) absorption [32] α_p, and coupling β, are given by

$$\alpha_p = \frac{\alpha_0}{2[1+(\Delta/\Gamma)^2]}\left(\frac{1+U_b+\mathcal{I}_m/2}{\sqrt{1+U_b}\{1+U_b+\mathcal{I}_m\}^{3/2}}\right), \tag{64}$$

$$\beta = \frac{\alpha_0}{4(1+(\Delta/\Gamma)^2)}\left(\frac{(i-\Delta/\Gamma)\mathcal{I}_m}{\sqrt{1+U_b}\{1+U_b+\mathcal{I}_m\}^{3/2}}\right), \tag{65}$$

and

$$\sigma^2 = |\beta|^2 - \alpha_p^2. \tag{66}$$

We note that in deriving the above expression for R, we have assumed that both $\mathcal{I}_m$ and U_b are constant throughout the medium, which we comment further on in Sec. IV.

IV. RESULTS FOR BACKGROUND RADIATION

In general we must obtain the background radiation term U_b required for our four-wave mixing result, by solving the radiative transfer problem numerically, using the formal solution Eq. (35). That solution is in fact implicit, since $\bar{\kappa}_\omega$ and $\bar{j}_\omega$ themselves depend on U_b. In addition, evaluation of $I_\omega^{\rm tot}$ (and hence U_b) at any given point requires, in principle, that $I_\omega(\rho,\eta)$ be calculated along each of the different paths that intersect at that point. In order to make the transfer problem tractable, we shall assume that the background radiation is constant throughout the medium, and use as an appropriate value of $I_\omega^{\rm tot}$ a conservative estimate for the central regions of the cylinder. We obtain this value by assuming that the distance η along every path is r_0, and we use

$$I_\omega^{\rm tot} \approx \int_{4\pi} I_\omega(\rho,\eta=r_0)\,d\Omega. \tag{67}$$

We note that the assumption of a constant background radiation field is consistent with our treatment of DFWM in Sec. III. Furthermore, we expect this to be a reasonable assumption in the central regions, where most of a probe beam path is likely to be.

Numerical results for U_b

We can now obtain U_b by solving Eq. (35) self-consistently for I_ω, by iteration. Assuming first that $U_b = 0$ in $\bar{\kappa}_\omega$ and $\bar{j}_\omega$, we evaluate I_w using Eq. (35) to obtain a first value for U_b using Eq. (44). The value of U_b produced is then used to improve $\bar{\kappa}_\omega$ and $\bar{j}_\omega$, until a self-consistent solution for I_w is obtained. In practice this takes only a few iterations.

In the development of I_ω both $\bar{j}_\omega$ and $\bar{\kappa}_\omega$ play a vital role, and the frequency dependence of these coefficients for a range of values of $I_{\rm max}$, both on and off resonance, is shown in Fig. 4 and Fig. 5, with $U_b = 0$. The modification caused by background radiation is illustrated in Fig. 6, where the functions $\bar{j}_\omega$ and $\bar{\kappa}_\omega$ are plotted in the absence of background radiation, as well as with a value of U_b appropriate to the pump intensity (and a cylinder radius $r_0 = 10/\alpha_0$). From a comparison of Figs. 4–6 with Figs. 2 and 3 we see that $\bar{j}_\omega$ and $\bar{\kappa}_\omega$ preserve the general features of j_ω and κ_ω calculated near the antinodes of the pumps' standing wave, although the peaks Rabi shifted to either side of the pump frequency are broadened due to the varying intensity across the pumps' standing wave.

These features are reflected also in the spectral profile of I_ω. For the resonant pump case, $I_\omega^{\rm tot}$ is calculated by our iterative procedure and is plotted in Fig. 7 as a function of the scattered frequency Δ_s for different values of $I_{\rm max}$ and for two different values of $\alpha_0 r_0 = 50$. Several

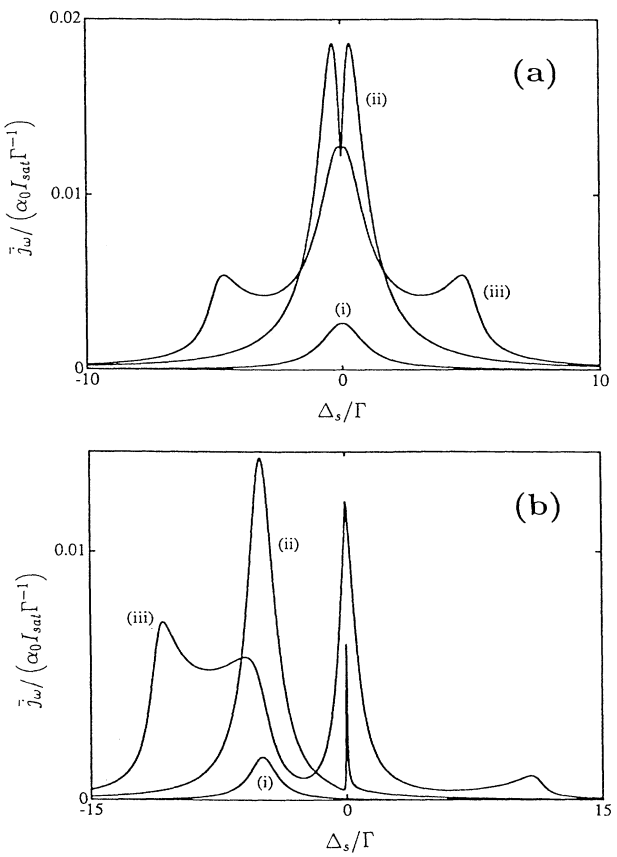

FIG. 4. The net emission coefficient $\bar{j}_\omega$ for (a) $\Delta = 0$ and (b) $\Delta = 5\Gamma$, with antinode intensities (a): (i) $I_{\rm max} = 0.25$, (ii) $I_{\rm max} = 25$, (iii) $I_{\rm max} = 2500$, and (b): (i) $I_{\rm max} = 4$, (ii) $I_{\rm max} = 100$, (iii) $I_{\rm max} = 10\,000$, corresponding in each case to the Rabi frequencies in Fig. 2, with $\gamma = 0.01\Gamma$.

important features are apparent from these curves. The I_ω profiles for finite r_0 are approximately Lorentzian or, for $\Omega \gtrsim \Gamma$, the sum of Lorentzians. For a given value of r_0, we see that as $I_{\max}$ first increases, the single peak of I_ω is enhanced near line center, and the bandwidth decreases. This behavior reflects the development of $\bar{j}_\omega$ (which increases near the center), and $\bar{\kappa}_\omega$ (which decreases). As $I_{\max}$ continues to increase, I_ω develops a dip at line center, which is simply the manifestation of the Rabi sidebands beginning to develop in $\bar{j}_\omega$, and overall, I_ω begins to saturate although the far wings remain Lorentzian. Comparing Fig. 7(a) with Fig. 7(b) shows that, as the cylinder radius increases, the bandwidth of the background intensity distribution also increases. The reason is that the absorption length is longer in the wings, and at long path lengths radiation continues to build in the wings while at line center it is close to its asymptotic intensity. For given $I_{\max}$, the integrated intensity $\int I_\omega d\omega$ will thus grow with r_0. For off-resonant pumps, at the intensities considered in this paper, most of the scattered radiation I_ω appears in a peak near the atomic frequency, and its bandwidth behaves in a similar way to the central peak in the on-resonant case. The secondary and narrow peak that occurs at the laser frequency may be enhanced by the gain that $\bar{\kappa}_\omega$ can possess in this region, but for all cases considered in this paper, the gain length is sufficently long compared to r_0 that the contribution to the integrated intensity is negligible. It is worth noting that the asymptotic intensity distribution in the wings, $\bar{j}_\omega/\bar{\kappa}_\omega$ [see Eq. (28)] is constant in ω [see Eq. (24) and Eq. (34)], but the far wings of I_ω will always be Lorentzian in a finite medium because the asymptotic distance can never be reached.

In order to obtain a value for U_b we fit Lorentzians to the I_ω profiles to give the bandwidths and band centers required in Eq. (44) or Eq. (56). On resonance we use a three Lorentzian fit, while off resonance a two Lorentzian fit is appropriate. In practice at pump powers such that $\Omega < \Gamma$, a single Lorentzian dominates the fit. We note that in some cases where r_0 is large, a flat region may develop in the near wings [before the final $(\Delta + \Delta_s)^{-2}$ falloff in the far wings] because the medium is optically thick in this region. However, such situations are not of interest in this paper as the pump beams will be weak and the "constant pump beams" approximation will fail.

Results obtained for the bandwidth of the main peak using this fitting procedure are summarized in Fig. 8, where contours of the bandwidth of I_ω^{tot} are plotted as

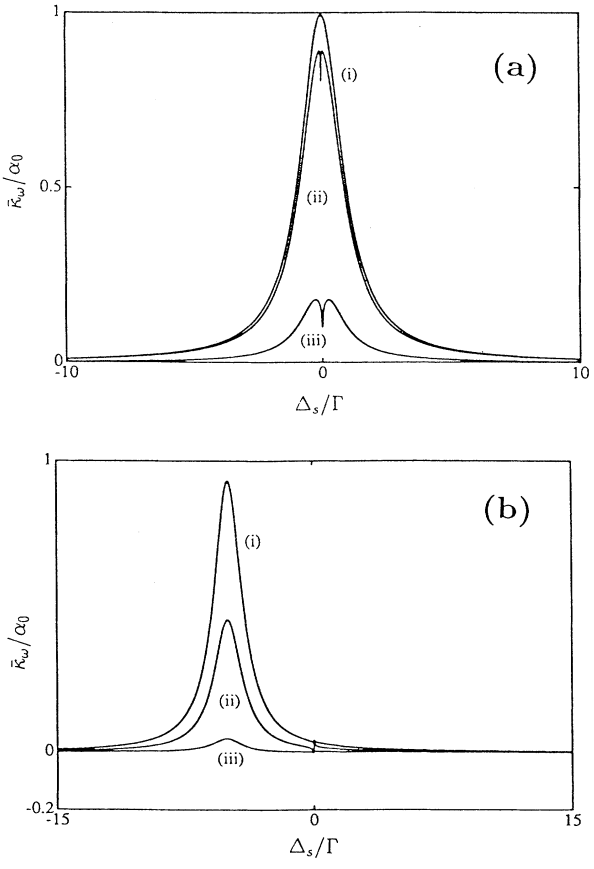

FIG. 5. The average absorption coefficient $\bar{\kappa}_\omega$ for (a) $\Delta = 0$ and (b) $\Delta = 5\Gamma$, with antinode intensities (a): (i) $I_{\max} = 0.01$, (ii) $I_{\max} = 0.25$, (iii) $I_{\max} = 25$, and (b): (i) $I_{\max} = 4$, (ii) $I_{\max} = 100$, (iii) $I_{\max} = 10\,000$, corresponding in each case to the Rabi frequencies in Fig. 3, with $\gamma = 0.01\Gamma$.

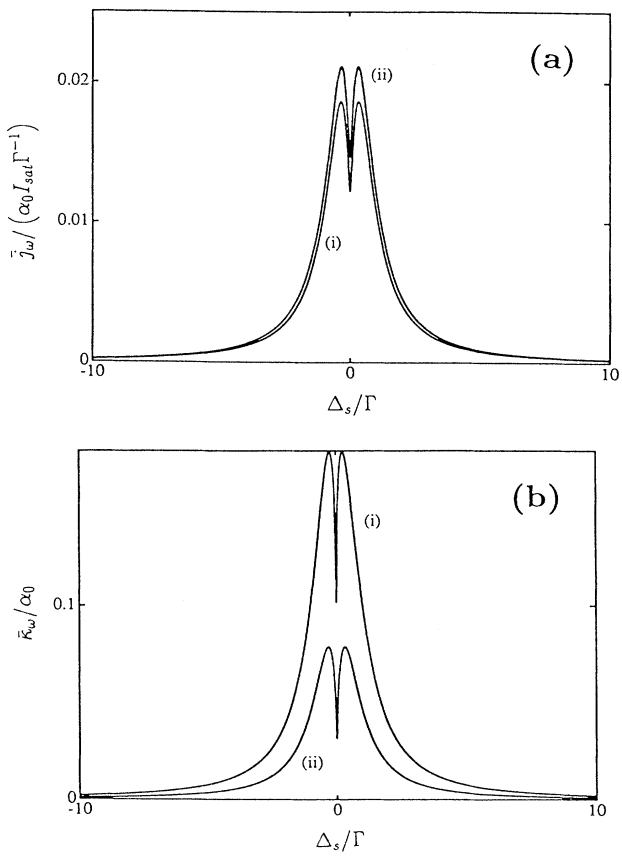

FIG. 6. Modification to the coefficients (a) $\bar{j}_\omega$ and (b) $\bar{\kappa}_\omega$ caused by U_b. All coefficients are calculated with $\Delta = 0$, $I_{\max} = 25$, $\gamma = 0.01$, but curves (i) have $U_b = 0$, and curves (ii) have $U_b = 3.4$.

a function of $I_{\max}$ and r_0 (at pump resonance). For the regime covered by this plot, $I_\omega^{\rm tot}$ has only one significant peak. The property noted above, that the bandwidth increases with cylinder radius r_0 and decreases with the pump intensity $I_{\max}$, is clearly evident, as also is the fact that the bandwidth tends to Γ for either $I_{\max}$ large, or r_0 small. In Fig. 9 we plot the behavior of U_b with increasing pump intensity. We see that for off-resonant pumps (dashed lines) the effective background intensity is diminished at higher effective pump intensities compared to the case for resonant pumps (solid lines).

Validity regime

The simplified form of the atomic response, Eq. (50), on which our DFWM treatment is based, is valid provided the conditions given in Eq. (38), Eq. (47), and Eq. (48) relating the bandwidth and mean Rabi frequency of the background radiation are satisfied. For strong homogeneous broadening ($\Gamma \gg \gamma$), we need consider only Eq. (47), since we have seen from Fig. 8 that the bandwidth b is always larger than (or nearly equal to) Γ. From numerical calculations, we have found in the resonant case that for $I_{\max} > 1$, the quantity $\overline{\Omega}_c^2/(b\Gamma)$ increases with $I_{\max}$ and with r_0 reaching a value of about

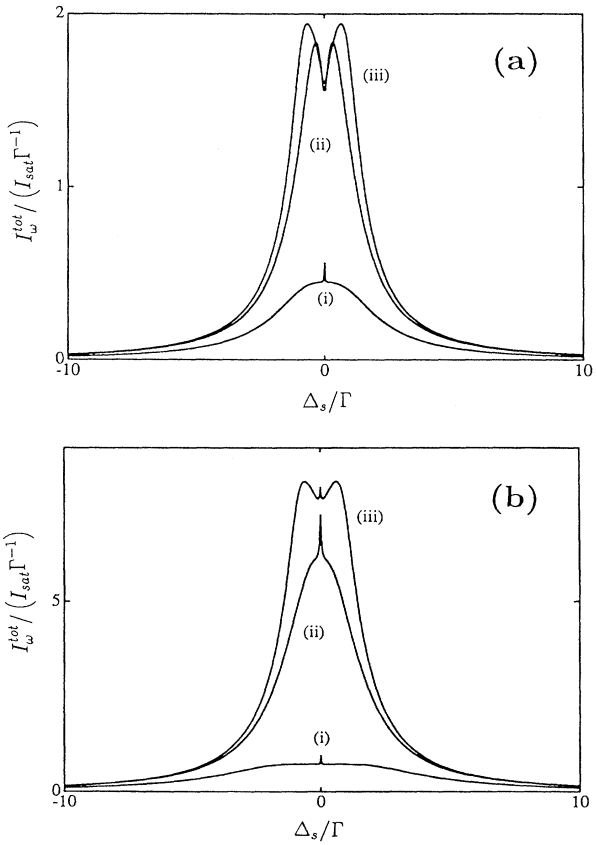

FIG. 7. Spectral profile of the total scattered intensity $I_\omega^{\rm tot}$, for $\Delta = 0$. In both (a) where $\alpha_0 r_0 = 10$, and (b) where $\alpha_0 r_0 = 50$, the antinode intensities are (i) $I_{\max} = 1$, (ii) $I_{\max} = 25$, and (iii) $I_{\max} = 100$.

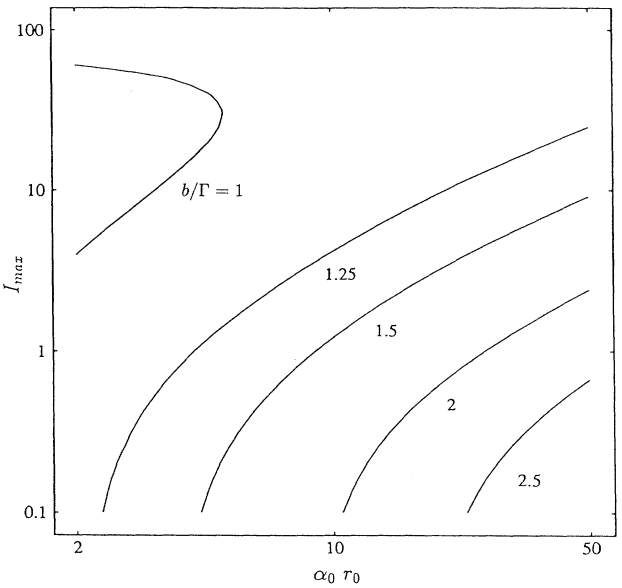

FIG. 8. Contours of the bandwidth b of $I_\omega^{\rm tot}$, for $\Delta = 0$, on a plot of $I_{\max}$ vs r_0.

0.1 at $I_{\max} = 10^3$ and $r_0 = 50$. Thus, for the purposes of this paper, the validity criterion Eq. (47) is met comfortably.

The assumption we made in Sec. II that the standing wave antinode intensities are approximately constant puts a lower limit on the intensity of the pumps for a given cylinder length ℓ. A strong coherent field suffers a much smaller fractional loss of amplitude with distance than a weak coherent field, and so the sum of forward and backward fields is more nearly constant for strong pumps than for weak. This property, which arises because of saturation, can be shown by numerically solving the coupled coherent propagation equations for the forward and backward pumps, and calculating the coefficient of variation (the ratio of rms deviation to mean) of the antinode in-

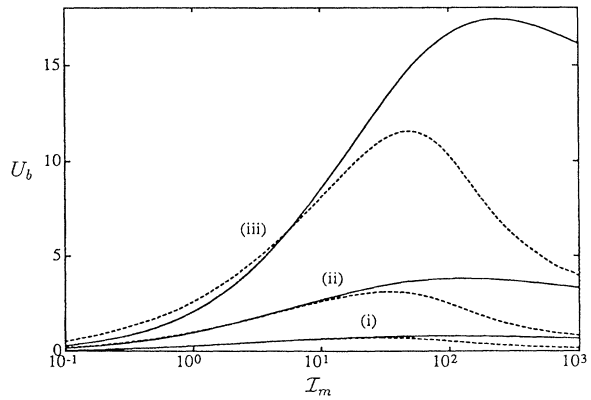

FIG. 9. Dependence of the background field saturation parameter U_b on the effective pump intensity $\mathcal{I}_m = I_{\max}/[1 + (\Delta/\Gamma)^2]$, for the case of resonant pumps (solid lines), and for pump-atom detuning $\Delta = 5\Gamma$ (dashed lines).

tensities throughout the standing wave. Since we intend this calculation to be indicative rather than quantitative, we have neglected the effect of the background radiation on the pump propagation, although this could be easily included [15]. In Fig. 10 we summarize the results from many such calculations by plotting the coefficient of variation against the average value of $I_{\max}$ for given cylinder length ℓ. From this figure we see for example that the "constant pump beams" approximation will be accurate to within 10% for a cylinder of length $10\alpha_0{}^{-1}$ provided $I_{\max} \gtrsim 10$. Inclusion of the background radiation would improve the accuracy, since it reduces the absorption.

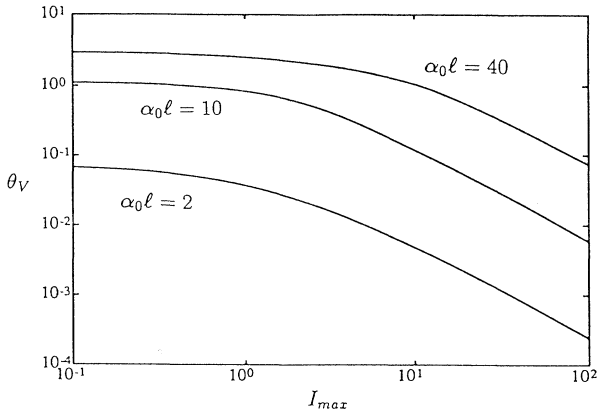

FIG. 10. Logarithmic plot of θ_V, the coefficient of variation of the antinode pump intensity $I_{\max}$, as a function of $I_{\max}$, for $\Delta = 0$ and three different cylinder lengths.

Analytic estimate of U_b

The behavior of U_b at large pump intensities can be characterized analytically. In this regime the average absorption coefficient has become sufficiently small that the medium is optically thin for all the scattered radiation, i.e.,

$$\bar{\kappa}_\omega r_0 \ll 1, \tag{68}$$

across the whole profile. Under this condition the background intensity is given by Eq. (36), and [using Eq. (67)] we can approximate $I_\omega^{\rm tot}$ by

$$I_\omega^{\rm tot} \approx 4\pi r_0 \bar{j}_\omega \tag{69}$$

$$\approx 4\pi r_0 \frac{1}{\lambda_\rho}\int_0^{\lambda_\rho} j_\omega(\rho,\eta)\,d\eta. \tag{70}$$

Integrating this expression over all frequencies we find [by interchanging the order of integration and using Eq. (19) and Eq. (21)]

$$\int_{-\infty}^{\infty} I_\omega^{\rm tot}\,d\omega \approx \alpha_0 r_0 I_{\rm sat}\left(1 - \frac{1}{\sqrt{(1+U_b)(1+U_b+\mathcal{I}_m)}}\right), \tag{71}$$

where we have used the strong broadening limit to put $f_{\rm inc} = 1$. The widths, weights, and frequency offsets of the Lorentzians constituting I_ω (and needed to complete the calculation of U_b), can be estimated from our knowledge of j_ω. For resonant pumps, I_ω is represented by a single Lorentzian centered on the atom frequency and with bandwidth $b \approx \Gamma$, provided $\Omega \le \Gamma$. When $\Omega \ge \Gamma$, half the spectral weight appears in sidebands of width $b \approx \Gamma/2$ displaced from the atomic frequency by the Rabi frequency, which we shall estimate from its rms value in the standing wave, i.e., $\Delta_c^2 \approx \gamma\Gamma I_{\max}/2$. Thus, using Eq. (56), we find the value of U_b for resonant pumps is

$$U_b \approx \frac{\alpha_0 r_0}{4}\left(1 + \frac{1}{1+I_{\max}\gamma/3}\right)\left(1 - \frac{1}{\sqrt{(1+U_b)(1+U_b+I_{\max})}}\right) \quad (\Delta = 0). \tag{72}$$

For off-resonant pumps ($\Delta > \Gamma$), the spectral character of I_ω is sufficiently different from the resonant case that the corresponding expression for U_b cannot be obtained by simply replacing $I_{\max}$ by $\mathcal{I}_m$ in Eq. (72). For $\Omega \le |\Delta|$, most of the spectral weight is in the sideband nearest the atomic frequency, but a band-center offset and a broadening of I_ω (which occur because of the intensity dependent shift of the sideband) contribute to lowering U_b. In the limit of large Ω, ($\Omega \gg \Delta$), half the spectral weight shifts to the central peak at $\Delta_s = 0$, giving a band center offset $\Delta_c = \Delta$, and consequently (neglecting the outer sidebands),

$$U_b \approx \frac{\alpha_0 r_0}{4}\frac{1}{1+\Delta^2/4\Gamma^2}\left(1 - \frac{1}{\sqrt{(1+U_b)(1+U_b+\mathcal{I}_m)}}\right) \quad (\Omega \gg \Delta > \Gamma). \tag{73}$$

Expressions (72) and (73) for U_b are, as expected, implicit, but in the case of an optically thin medium [see Eq. (68)] the square root term represents a small correction to the remaining term, and to good approximation we may write

$$U_b \approx \begin{cases} \frac{\alpha_0 r_0}{4}\left(1 + \frac{1}{1+I_{\max}\gamma/3}\right) & (\Delta = 0) \quad (74) \\ \frac{\alpha_0 r_0}{4}\frac{1}{1+\Delta^2/4\Gamma^2} & (\Omega \gg \Delta > \Gamma). \quad (75) \end{cases}$$

A characteristic value of the pump intensity at which Eq. (74) (for resonant pumps) may be applied can be obtained using our estimate Eq. (30) for the maximum value of $\bar{\kappa}_\omega$ in Eq. (68) giving

$$\sqrt{(1+U_b)(1+U_b+I_{\max})} \gg \alpha_0 r_0, \tag{76}$$

although in practice

$$\sqrt{(1+U_b)(1+U_b+I_{\max})} > 2\alpha_0 r_0 \quad (77)$$

is sufficient. Now approximating U_b by the value $\alpha_0 r_0/4$, we find the (resonant) pump intensity above which Eq. (74) applies is given roughly by

$$I_{\max} > \begin{cases} 12\alpha_0 r_0 - 16, & 2 < \alpha_0 r_0 < 5 \quad (78) \\ 15\alpha_0 r_0 - 40, & 10 < \alpha_0 r_0 < 50. \quad (79) \end{cases}$$

V. RESULTS FOR DFWM

The reflectivity R that we have derived in Eq. (63) for DFWM in the presence of the background field can now be evaluated using the values of U_b obtained numerically in the preceding section. Beginning with the resonant case, we plot with solid lines in Fig. 11(a) curves of R versus the pump intensity for several different interaction lengths L, for a cylinder of radius $2\alpha_0^{-1}$. The dashed curves give the reflectivity in the absence of background radiation and are identical to those given previously by Abrams *et al.* [33]. In Fig. 11(b) similar curves are presented, but now for a cylinder of radius $10\alpha_0^{-1}$. The salient feature of these two figures is that the reflectivity is diminished by the scattered background radiation; at $r_0 = 10\alpha_0^{-1}$ and $L = 10\alpha_0^{-1}$, for example, the background radiation reduces the maximum reflectivity by approximately 77%. The fractional decrease in reflectivity is largest with large r_0, has only a weak dependence on the probe path length L, and is relatively insensitive to the pump intensity. The decrease in R is governed by the value of the background radiation term U_b which is strongly dependent on r_0 since a larger cylinder traps more radiation. On the other hand, U_b changes little with pump intensity (for the values of r_0 in these figures) when $I_{\max} > 1$, and thus the depression of the reflectivity is also almost independent of the pump intensity [see also Eq. (93)].

In Fig. 12 which corresponds exactly to Fig. 11 but with $\Delta = 5\Gamma$, the effect of pump detuning is shown. Again we see diminishment of reflectivity, with a strong dependence on r_0 and little dependence on L. At the peak values of reflectivity (which occur in the region $1 < \mathcal{I}_m < 10$) the fractional decrease is of the same order, or larger, than for the resonant case. This somewhat surprising result arises because, at these intensities, most of the scattered radiation is redistributed into a band centered on the atomic resonance, where it is most effective in interacting with nearby atoms. As $\mathcal{I}_m$ increases further, the redistributed radiation is pushed into bands

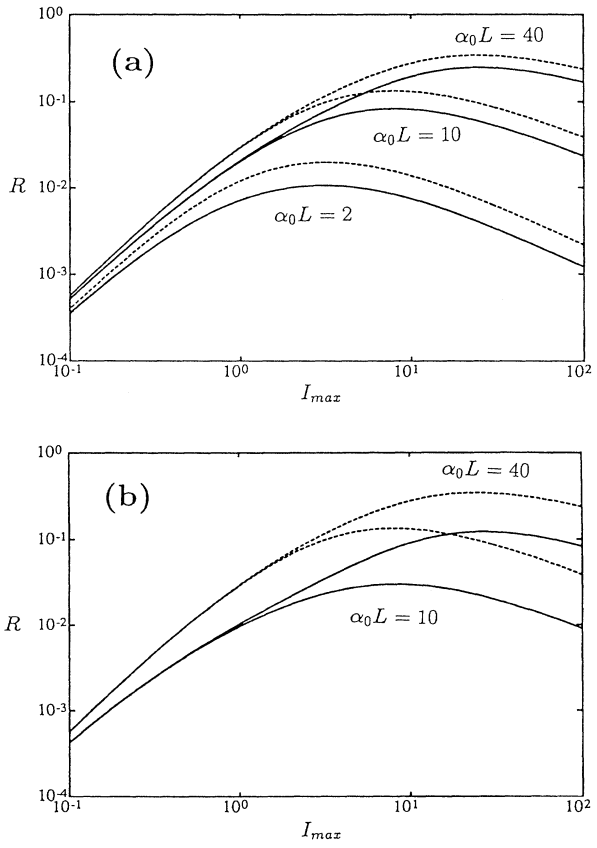

FIG. 11. Logarithmic plot of the reflectivity R against $I_{\max}$, for $\Delta = 0$, with (a) $\alpha_0 r_0 = 2$ and (b) $\alpha_0 r_0 = 10$. The theory including background radiation is plotted as solid lines while the standard theory [1] which neglects background radiation is plotted as dashed lines.

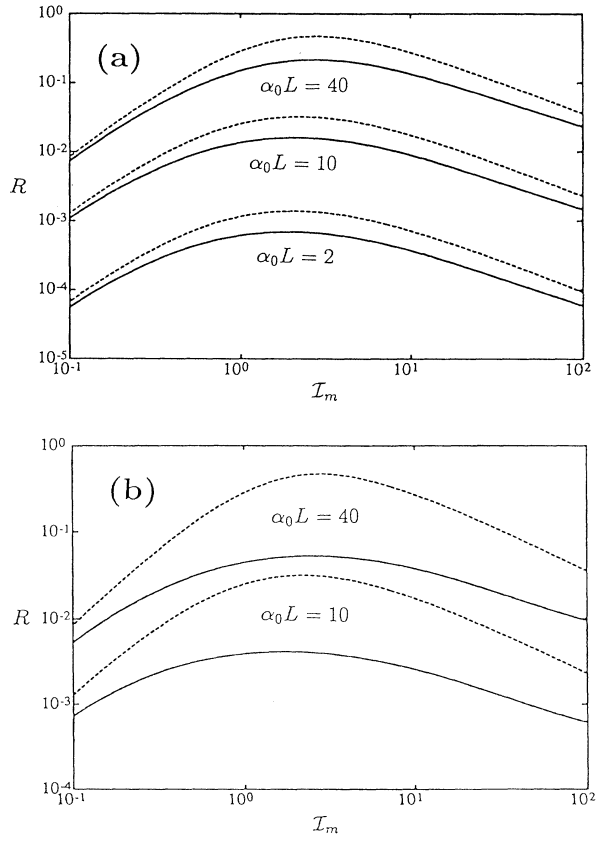

FIG. 12. Logarithmic plot of R against $I_{\max}$, as in Fig. 11 but with $\Delta = 5\Gamma$.

further away from the atomic resonance, which decreases U_b (see Fig. 9), and hence decreases the effect of the scattered radiation on the reflectivity. This can be seen clearly in the high intensity region of Fig. 12(b), where the dashed and solid curves begin to move closer together.

Approximate analytic forms for the reflectivity which give insight into this behavior can be found in the regime where $|\sigma L| \ll 1$, in which case Eq. (63) for R becomes

$$R \approx \left| \frac{\beta L}{1+\alpha_p L} \right|^2 . \tag{80}$$

This can be further simplified by noting that when $\mathcal{I}_m \gg 1$ and $U_b < \mathcal{I}_m$ (as it will be in regimes where the constant pump beam approximation is valid), α_p can be well approximated by

$$\alpha_p \approx \frac{\bar{\alpha}_0}{4\sqrt{(1+U_b)(1+\mathcal{I}_m)}}, \tag{81}$$

where

$$\bar{\alpha}_0 = \frac{\alpha_0}{[1+(\Delta/\Gamma)^2]}. \tag{82}$$

We can then write

$$R \approx \frac{\mathcal{I}_m^2[1+(\Delta/\Gamma)^2]}{4(1+U_b+\mathcal{I}_m/2)^2} \left| \frac{\bar{\alpha}_0 L}{\bar{\alpha}_0 L + 4\sqrt{(1+U_b)(1+\mathcal{I}_m)}} \right|^2 \quad (|\sigma L| \ll 1). \tag{83}$$

The validity condition for Eq. (83) can be given in a more explicit form provided the product $|\Delta|\mathcal{I}_m$ satisfies

$$\frac{|\Delta|}{\Gamma}\mathcal{I}_m < 1 + U_b, \tag{84}$$

since in this case a close upper bound on σ is given by

$$\sigma = \frac{i\bar{\alpha}_0}{2(1+U_b+\mathcal{I}_m)}. \tag{85}$$

The condition $|\sigma L| \ll 1$ thus becomes [when Eq. (84) is satisfied]

$$\bar{\alpha}_0 L \ll 2(1+U_b+\mathcal{I}_m). \tag{86}$$

In practice, it is unusual for both $\mathcal{I}_m$ and Δ to be large [see Eq. (31)], so that Eq. (86) provides a validity condition for Eq. (83) that covers many situations of interest. When Eq. (84) is violated, then broadly speaking, σ becomes real. Specifically, when

$$\frac{\Delta}{\Gamma}\mathcal{I}_m > 2\sqrt{(1+U_b)(1+U_b+\mathcal{I}_m)}, \tag{87}$$

σ is real, and we can approximate it by

$$\sigma \approx \frac{\bar{\alpha}_0|\Delta|}{4\Gamma\sqrt{(1+U_b)}} \frac{\mathcal{I}_m}{\{1+U_b+\mathcal{I}_m\}^{3/2}}. \tag{88}$$

Thus the condition for Eq. (83) to hold in the regime where Δ is nonzero and $\mathcal{I}_m$ is large [i.e., Eq. (87)] can be written approximately as

$$\bar{\alpha}_0 L \frac{|\Delta|}{\Gamma} < \frac{4}{\mathcal{I}_m}\sqrt{(1+U_b)}\{1+U_b+\mathcal{I}_m\}^{3/2}. \tag{89}$$

It is also possible to give an approximate value for R in the regime $|\sigma L| > 1$, in the case where the product $|\Delta|\mathcal{I}_m$ satisfies the condition Eq. (84), since then σ is pure imaginary, and $\cos(|\sigma|L) \to e^{|\sigma|L}/2$ and $\sin(|\sigma|L) \to -e^{|\sigma|L}/2i$. The reflectivity can then be written approximately as

$$R \approx \left| \frac{i\beta}{i(|\sigma|+\alpha_p)} \right|^2 , \tag{90}$$

and noting that $|\sigma| \sim \alpha_p$ in the regime where Eq. (84) holds, we may write

$$R \approx \frac{1}{4}\left|\frac{\beta}{\alpha_p}\right|^2 = \frac{\mathcal{I}_m^2[1+(\Delta/\Gamma)^2]}{16(1+U_b+\mathcal{I}_m/2)^2} \left(|\sigma L| > 1, \ \frac{\Delta}{\Gamma}\mathcal{I}_m < 1+U_b \right). \tag{91}$$

Once σ becomes real, which it does with finite Δ if $\mathcal{I}_m$ is sufficiently large, then for $\sigma L > \pi/2$, the reflectivity in Eq. (63) will exhibit resonances [17]. At these resonances, the assumption of nondepletion of the pump is no longer valid, and the standard FWM theory must be modified [8]. We note that all the results we have presented (Figs. 11 and 12) are well outside the regime where resonances might occur.

The form in Eq. (83) therefore allows us to make a simple comparison between the reflectivity R predicted by our theory and the reflectivity R_0 of the standard theory ($U_b = 0$), which will be useful over a wide practical range of parameters. Using Eq. (83) we find

$$\frac{R}{R_0} \approx \left(1+\frac{U_b}{1+\mathcal{I}_m/2}\right)^{-2} \times \left(1+\frac{\sqrt{1+U_b}-1}{1+\bar{\alpha}_0 L/(4\sqrt{1+\mathcal{I}_m})}\right)^{-1}, \tag{92}$$

from which it is clear that the background radiation always acts to decrease the reflectivity. In the regime where $\mathcal{I}_m$ is large (i.e., $\mathcal{I}_m \gg U_b$, and $\sqrt{\mathcal{I}_m} \gg \bar{\alpha}_0 L/4$), the reflectivity ratio takes the simple form

$$\frac{R}{R_0} \approx \frac{1}{\sqrt{1+U_b}}, \tag{93}$$

which shows that the fractional decrease in reflectivity depends mainly on the level of the background radiation, as discussed in connection with the figures at the beginning of this section. A final simple approximate form that has explicit dependence on the system parameters can be obtained by substituting the asymptotic expressions for U_b [Eq. (74) and Eq. (75)] into Eq. (93).

VI. CONCLUSION

We have formulated a model to quantitatively investigate how the generation of a conjugate beam in near-resonant DFWM is affected by radiation scattered from

the pump beams. The main assumptions we have made to ensure tractability are (i) the pump beams have constant amplitudes and plane wave fronts in a cylinder of radius r_0, (ii) collision broadening is dominant and atomic motion is ignored, and (iii) directional and polarization effects in the scattering process are neglected, and the scattered radiation is assumed to be homogeneous and isotropic. Within this framework the spectral intensity distribution of the scattered radiation is obtained and shown to be well characterized as a sum of chaotic Markovian fields. These fluctuating background fields act on the atomic media in concert with the coherent laser fields and modify the optical dipole induced by the coherent fields. The modification does not have a simple physical interpretation in terms of new decay or dephasing rates but, nevertheless, over a broad regime where a decorrelation approximation is valid, can be expressed via a single parameter U_b which incorporates the energy of the fluctuating field together with bandwidths and frequency offsets from the atomic resonance. In addition to detailed numerical solutions for the DFWM reflectivity, we have also given simple analytic approximations for the scattered radiation term U_b and the reflectivity, which help illuminate the underlying mechanisms of the system.

Our results clearly bear some relationship to the work of Cooper *et al.* [2] who considered fluctuating pump (and probe) fields, but certain important differences emerge. They find that at some pump intensities the reflectivity is lowered compared to the monochromatic case, while at other intensities it may be increased. For many cases they consider, they find the fluctuations cause the peak of the reflectivity curve to move to higher intensities because of the effect of the fluctuations. In our case the reflectivity is always reduced by the scattered field for any given pump intensity, and the position of the peak reflectivity barely changes. Furthermore, while the reflectivity in their case falls as $I^{-3/2}$ at high intensities, in our case it falls as I^{-1} [see Eq. (83)]. The underlying difference is that in our case the fluctuating field becomes more or less constant above a certain pump intensity, whereas in their case the fluctuations are intrinsic to the pump field.

A simple picture for the way in which the scattered field affects the FWM process can be given in terms of the spatial modulation of the polarization formed by the standing wave field of the pump beams. The probe beam can be thought of as reading the spatial harmonic structure of the grid and, in the decorrelation approximation, the grid has a spatial form which follows the population inversion [see Eq. (49)]. In the absence of a background field, the polarization will be saturated across most of the standing wave, except for a very sharp feature corresponding to the zero value of the coherent field at the nodes. When a background field is present, it reduces the inversion at the nodes, thus reducing the sharpness of the polarization feature and hence altering the harmonic structure of the grid. In this paper, where we have considered only degenerate FWM, we have shown that the harmonic content at the pump frequency is always reduced by the background field.

ACKNOWLEDGMENTS

We wish to thank Dr. P. Ewart for encouraging us to work on this problem, and for many helpful discussions. We are also grateful for helpful discussions with Dr. J. Cooper and Dr. L. Casperson.

APPENDIX

In this appendix we give some additional results and approximations to the emission and absorption coefficients, and quantify the validity regimes of the approximate forms. In the limit of well separated spectral lines ($\Omega' \gg \Gamma$), Eqs. (4)–(6) in Ref. [26] give explicit expressions for the widths and weights of the three Lorentzian components of j_ω. These expressions are still quite complicated, and so it is worth summarizing the main features here. The widths of the outer sidebands are of order Γ. At resonance the center peak has width Γ, but for $\Delta \neq 0$ the width is γ at low laser power, and Γ at high power. For strong collisional broadening ($\Gamma \gg \gamma$) and $\Omega \gg |\Delta|$, the three peaks are of same height, but the sidebands have width $\Gamma/2$ (i.e., half the width of the center peak). On the other hand, if $|\Delta| \gg \Omega$, for strong collisional broadening most of the scattered intensity is in the sideband nearest the atomic resonance frequency, with the relative weighting of the center Lorentzian being of order $\Omega^2/2\Delta^2$, and the relative weighting of the far sideband being of order $(\Omega^2/8\Delta^2)\left[\gamma/\Gamma + \Omega^2/(2\Delta^2\right]$.

It can also be shown directly from Eq. (11) that when

$$\frac{\Omega^2}{(\Delta+\Delta_s)^2+\Gamma^2} \ll 1, \tag{A1}$$

i.e., in the wings of the line or at sufficiently low laser power, the emission coefficient is well described by the form Eq. (23) apart from the region $|\Delta_s| < \Gamma$ (i.e., apart from the feature at the pump frequency). At very low pump power ($\Omega \leq \gamma$) the Lorentzian form Eq. (23) is accurate throughout the whole profile. For the off-resonant case ($\Delta \geq \Gamma$), Eq. (23) is a very good representation of j_ω, provided $\Omega \ll \Delta$, even in regions where Eq. (A1) is not satisfied, since the relative weights of the two other peaks (at $\Delta_s = 0$ and $\Delta_s = \Delta$) are negligible.

Equation (24) provides an off-resonant ($\Delta > \Gamma$) form of κ_ω that is useful over a wide parameter range. On resonance, κ_ω remains Lorentzian in the wings ($|\Delta_s| > \Omega$) where it can be approximated by

$$\kappa_\omega \underset{\Delta=0,|\Delta_s|>\Omega}{\longrightarrow} -\alpha_0 n\Gamma \frac{\Gamma}{\Delta_s^2+\Gamma^2}\left\{1+\frac{\Omega^2}{2\Gamma^2}\right\}. \tag{A2}$$

However, in the center region of the line, the absorption is suppressed, falling sharply near $|\Delta_s| = \Omega$, and may actually become negative (i.e., gain) in the regions near $|\Delta_s| = \Omega$ for large enough pump power ($\Omega > \Gamma$). At the exact line center ($\Delta_s = 0$), κ_ω takes the value

$$\kappa_\omega \underset{\Delta=0,\Delta_s=0}{\longrightarrow} -\alpha_0 n\left[1+\frac{|\Omega|^2}{\Gamma\gamma}\right]^{-1}, \tag{A3}$$

which is always positive, but may be very small. A line-center value for j_ω is also useful, and at resonance can be approximated by

$$j_\omega \underset{\Delta=0,\Delta_s=0}{\longrightarrow} = \frac{\alpha_0 I_{\rm sat} f_{\rm inc}}{8\Gamma\pi^2}\left[1+\frac{U_b-1}{1+U_b+2I}\right]. \tag{A4}$$

[1] R. L. Abrams, J. F. Lam, R. C. Lind, D. G. Steel, and P. F. Liao, in *Optical Phase Conjugation,* edited by R. A. Fisher (Academic, New York, 1983), Chap. 8.
[2] J. Cooper, A. Charlton, D. R. Meacher, P. Ewart, and G. Alber, Phys. Rev. A **40**, 5705 (1989).
[3] P. R. Berman, D. G. Steel, G. Khitrova, and J. Liu, Phys. Rev. A **38**, 252 (1988).
[4] R. G. DeVoe and R. G. Brewer, Phys. Rev. Lett. **50**, 1269 (1983).
[5] S. Singh and G. S. Agarwal, J. Opt. Soc. Am. B **5**, 254 (1988).
[6] K. Burnett, J. Cooper, R. J. Ballagh, and E. W. Smith, Phys. Rev. A **22**, 2005 (1980).
[7] H. Wang and D. G. Steel, Phys. Rev. A **43**, 3823 (1991).
[8] W. P. Brown, J. Opt. Soc. Am. **73**, 629 (1983).
[9] R. McGraw, Phys. Rev. A **42**, 2235 (1990).
[10] R. McGraw, Phys. Rev. A **45**, 3250 (1992).
[11] E. A. Milne, J. Lond. Math. Soc. **1,** 40 (1926).
[12] J. Huennekens and A. Gallagher, Phys. Rev. A **28**, 238 (1983).
[13] T. Colbert and J. Huennekens, Phys. Rev. A **41**, 6145 (1990).
[14] H. A. Post, Phys. Rev. A **33**, 2003 (1986).
[15] A. W. McCord, R. J. Ballagh, and J. Cooper, Opt. Commun. **68**, 375 (1988).
[16] W. Lange, G. Ankerhold, M. Schiffer, D. Mutschall, and T. Scholz, XVIII International Quantum Electronics Conference, Vienna, 1992 (Institut für Nachrichtentechnik der TU Wien, Vienna, 1992).
[17] R. L. Abrams and R. C. Lind, Opt. Lett. **2**, 94 (1978); Errata: *ibid.* **3**, 205 (1978);
[18] Zoller *et al.* [19] have shown that a field consisting of a number of uncorrelated modes becomes a chaotic field as the number of modes becomes large.
[19] P. Zoller, G. Alber, and R. Salvador, Phys. Rev. A **24**, 398 (1981).
[20] A. W. McCord, Ph.D. thesis, University of Otago, 1988 (unpublished).
[21] S. Chandrasekhar, *Radiative Transfer* (Dover, New York, 1960), Chap. 1.
[22] Although a more detailed model could be constructed to include a spatial Gaussian profile of the pump beams, we can, by adjusting r_0 in our model, account for any significant difference that the Gaussian profile would effect on the buildup of background radiation in the four-wave mixing region.
[23] This approximation enforces complete redistribution of the transferred radiation.
[24] We appreciate the use of the software developed by A.W. McCord for his Ph.D. thesis [20] in validating this point.
[25] B. R. Mollow, Phys. Rev. A **5**, 2217 (1972).
[26] B. R. Mollow, Phys. Rev. A **15**, 1023 (1977).
[27] J. H. Lee, J. J. Song, M. A. F. Scarparo, and M. D. Levenson, Opt. Lett. **5**, 196 (1980).
[28] R. W. Boyd, M. G. Raymer, P. Narum, and D. J. Harter, Phys. Rev. A **24**, 411 (1981).
[29] When κ_ω is negative, Eq. (26) is still correct but Eq. (28) is no longer an asymptote. For cases considered in this paper, such gain regions have negligible contribution to the integrated intensity; see also Sec. IV.
[30] P. Zoller, Phys. Rev. A **20**, 1019 (1979).
[31] A. T. Georges, Phys. Rev. A **21**, 2034 (1980).
[32] In principle the probe absorption given by Eq. (64) should agree with $\bar{\kappa}_\omega/2$ at $\Delta_s = 0$. Our two forms, though not identical, are numerically very close, confirming the decorrelation approximation used in deriving $\bar{\kappa}_\omega$.
[33] Compare with Abrams *et al.* [1], Fig. 4. Notation: $\alpha_{0\text{Abrams}} = \frac{1}{2}\alpha_0$, $(I/I_{\text{sat}})_{\text{Abrams}} = \frac{1}{2}I_{\max}$.